Research Square

Preprints are preliminary reports that have not undergone peer review.
They should not be considered conclusive, used to inform clinical practice,
or referenced by the media as validated information.

Cross-lineage single-cell and spatial analysis identifies an endothelial NF-kB-CCL2 axis coupled to myeloid IL1B in sarcoma and carcinoma

Saiyang Li

lsy2866139350163.com

Jiamusi Maternal and Child Health Hospital

Research Article

Keywords: CCL2, CCR2, NF-kB, tumor microenvironment, sarcoma, single-cell analysis

Posted Date: November 12th, 2026

DOI: https://doi.org/10.21203/rs.3.rs-11035851/v1

License: This work is licensed under a Creative Commons Attribution 4.0 International License.
Read Full License

Additional Declarations: No competing interests reported.

Cross-lineage single-cell and spatial analysis identifies an endothelial NF-kB-CCL2 axis coupled to myeloid IL1B in sarcoma and carcinoma

Saiyang Li1,*

1 Jiamusi Maternal and Child Health Hospital, Jiamusi, Heilongjiang, China

*Correspondence: Saiyang Li, Jiamusi Maternal and Child Health Hospital, Jiamusi, Heilongjiang, China.
Email: lsy286613935@163.com

ORCID: 0009-0004-2665-4245

Abstract

CCL2-CCR2 signaling recruits myeloid cells in cancer, but the CCL2-producing compartments and upstream inflammatory programs are usually studied within one tissue context. We integrated five human single-cell cohorts spanning UPS sarcoma, oral SCC, TNBC, colorectal cancer, and NSCLC; 12 Visium spatial samples; LIANA and CellChat communication analyses; patient-level pseudobulk meta-analysis; NicheNet inference; DepMap and PRISM screens; and external bulk validation in TCGA-SARC and GSE202361. CCL2 was produced mainly by fibroblast/CAF, endothelial, and myeloid cells, whereas malignant epithelial CCL2 positivity was low; UPS malignant mesenchymal cells showed higher CCL2 positivity, although this sarcoma comparison was small. CCR2 was sparse and concentrated in myeloid, B/plasma, and T/NK compartments. LIANA and CellChat supported fibroblast/CAF-to-myeloid and endothelial-to-myeloid CCL2-CCR2 axes across all five cohorts. Endothelial NFKB_TARGETS was the most stable patient-level program associated with CCL2 (pooled rho = 0.680, p = 0.00021, I2 = 0), and myeloid IL1B was the most consistent upstream candidate (rho = 0.452, p = 0.0335, I2 = 0). Spatial NF-kB-high regions were myeloid-enriched, but CCL2 was not axis-specific. External UPS cohorts supported NFKB_TARGETS-CCL2 and NFKB_TARGETS-IL1B associations, with attenuation of the CCL2 relationship after composition adjustment. These findings support a microenvironment model centered on myeloid IL1B, endothelial NF-kB, and CCL2 without establishing causality.

Keywords: CCL2; CCR2; NF-kB; tumor microenvironment; sarcoma; single-cell analysis

Introduction

CCL2 recruits CCR2-expressing monocytes and contributes to the composition and function of the tumor microenvironment. In many tumors, CCL2 has been interpreted primarily as a tumor-cell-derived chemokine, but single-cell studies show that stromal and immune cells can also be dominant sources. The relative contribution of malignant, endothelial, fibroblastic, and myeloid compartments is therefore context dependent, and bulk measurements cannot identify the sender cell that drives a CCL2-associated state.

NF-kB is a canonical regulator of inflammatory gene expression. Experimental studies in cancer and non-cancer systems connect NF-kB or NF-kB-associated inflammatory signaling to CCL2, but the strength and direction of this relationship can vary by cell type and disease. In NSCLC, PIM1-dependent NF-kB-CCL2 signaling has been linked to macrophage infiltration and anti-PD-1 response. Endothelial cells are an attractive but less frequently tested source of CCL2 because they can integrate myeloid cytokines and regulate leukocyte recruitment.

This study asked four questions. First, which malignant and stromal compartments produce CCL2 across sarcoma and carcinoma? Second, which cells express CCR2 and could receive the signal? Third, is NF-kB activity coupled to CCL2 at the patient level, and which program is most reproducible across cell types and datasets? Fourth, which upstream ligand and therapeutic axis is most consistent across communication, spatial, dependency, and clinical evidence? We addressed these questions with a cross-lineage integration designed to preserve donor-level uncertainty and to expose negative or non-specific findings rather than selecting only the strongest pooled association.

Methods

Study design and data sources

We performed an integrative analysis of public human tumor datasets. The single-cell discovery set comprised UPS sarcoma (GSE212527; two donors and 3,824 cells), oral SCC (CELLxGENE; 12 donors and 28,186 cells), TNBC stromal samples (CELLxGENE; four untreated donors and 18,976 cells), colorectal cancer (GSE132465; 23 tumor donors and 47,285 cells), and NSCLC (GSE127465; seven human tumor donors and 40,362 cells). Carcinoma cohorts contributed 46 donors and 134,809 cells. The spatial validation set comprised 12 Visium samples: four sarcoma samples from GSE212526, three treated ccRCC samples from GSE294006, and five squamous carcinoma samples from GSE321832.

External validation used the TCGA-SARC UPS/MFH/high-grade spindle-cell subset (44 samples; 14 OS events and 23 DFS events) from cBioPortal sarc_tcga_pub, and GSE202361, a neoadjuvant immune checkpoint blockade cohort in DDLPS and UPS. GSE202361 contained 64 bulk RNA-seq samples from baseline, on-treatment, surgery, and relapse time points; the baseline PD-versus-non-PD analysis used 23 samples.

Single-cell preprocessing and cell-type harmonization

Available complete-expression matrices were analyzed with harmonized cell-type labels. For LIANA and NF-kB analyses, raw counts were library-size normalized to 10,000 counts per cell and transformed with log1p. Cell-type labels were harmonized into malignant mesenchymal, malignant epithelial-like, malignant epithelial, epithelial, fibroblast/CAF, endothelial, perivascular, myeloid, T/NK, B/plasma, and mast compartments.

For cell-type summaries, CCL2 and CCR2 positivity were calculated within each donor and cell type. Donor-level summaries were preferred over pooled-cell tests for descriptive comparisons. The UPS sarcoma result remains limited to two donors.

OpenAI Codex was used to assist with code generation, data processing, statistical analysis, figure preparation, and manuscript drafting. The author reviewed and verified all analyses, numerical results, text, and final content.

LIANA and CellChat communication analysis

LIANA 0.1.9 was run with rank_aggregate and the consensus ligand-receptor resource. Cell types required at least 20 cells. The standard full-network analysis used expr_prop = 0.1; a targeted CCL2-CCR2 analysis used expr_prop = 0 and 1,000 permutations. Donor-level targeted analyses repeated the workflow within each eligible donor.

CellChat 2.1.2 was run independently with CellChatDB human and a targeted CCL2-CCR2 ligand-receptor pair. Because CCR2 was sparse, thresholdedMean was used with trim = 0.005, population.size = TRUE, and 20 bootstrap iterations. This analysis was exploratory and used to test direction, not to estimate calibrated communication probabilities.

NF-kB program scoring and patient-level meta-analysis

NF-kB activity was summarized with two gene sets after excluding CCL2 and CCR2: NFKB_CORE (NF-kB subunits, inhibitors, and feedback regulators; 12 genes) and NFKB_TARGETS (canonical downstream targets; 38 genes). AUCell scores were generated with decoupler 2.2.0. Donor-level Spearman correlations were calculated between the cell-type program score and CCL2 expression or CCL2-positive fraction. Dataset-level correlations were combined with Fisher-z random-effects meta-analysis.

Spatial neighborhood and null-model analysis

Each Visium sample retained spots with in_tissue = 1 and total counts of at least 500. For each spot, the mean of the six nearest neighbors was used to calculate neighborhood CCL2 and myeloid scores. The myeloid score was the mean normalized expression of CD68, CD163, LYZ, and PTPRC. Translation, rotation, and mirror null models preserved local spatial structure while disrupting the alignment between NF-kB and the target neighborhood field. Control axes included CCL3, CCL4, CCL5, CXCL8, CXCL9, CXCL10, CXCL12, CCR2, CCR5, CXCR3, and CXCR4.

NicheNet upstream inference

NicheNet 2.2.1.1 was run with the official v2 prior model and pseudobulk expression profiles from the five single-cell cohorts. Endothelial and myeloid cells were analyzed as receivers, using NFKB_TARGETS as the target gene set. Ligands were required to have at least 10% detection in a non-receiver compartment. Dataset-level ligand activities were summarized, and canonical ligands were tested for donor-level association between myeloid ligand expression and endothelial NFKB_TARGETS or CCL2.

Target dependency and compound sensitivity

DepMap Public 24Q4 Chronos gene-effect data were analyzed across 1,178 cell lines. PRISM Repurposing Public 24Q2 collapsed LFC data were analyzed for CCR2 antagonists, IKK/NF-kB compounds, and IL1/IRAK-related compounds by lineage. These screens evaluate cell-autonomous growth effects and cannot directly test microenvironment signaling.

External clinical validation

In TCGA-SARC, NFKB_TARGETS and NFKB_CORE scores were calculated from z-scored gene expression and tested with Cox models for OS and DFS. An exploratory non-negative least-squares deconvolution model used UPS single-cell marker signatures and adjusted survival models for endothelial and myeloid fractions.

In GSE202361, HGNC-mapped TPM values were used to score NFKB_TARGETS, NFKB_CORE, CCL2, IL1B, IL1R1, CCR2, TNF, and TNFRSF1A. Baseline PD was compared with non-PD (SD or PR) using non-parametric tests and age-adjusted logistic regression. GEO, BioSample, SRA, and Nature supplement metadata did not contain a verified GSM-to-Acc patient crosswalk, so the continuous hyalinization endpoint was not analyzed.

Statistical interpretation

Analyses were interpreted as exploratory unless explicitly identified as validation. Pooled Spearman estimates were reported with 95% confidence intervals, p values, and I2. Spatial p values from translation and rotation null models were interpreted with their known limitations. No analysis was interpreted as causal. Multiplicity was not uniformly controlled across discovery, spatial, and external analyses, and the results should therefore be viewed as hypothesis-generating.

Results

CCL2 is a multicellular stromal signal

Across five single-cell cohorts, CCL2-positive fractions varied by disease and cell type (Figure 2). CAF/fibroblast, endothelial, and myeloid cells were recurrent CCL2 sources in carcinomas. In NSCLC, myeloid cells contributed the largest share of CCL2-positive cells, whereas CAF/fibroblast and endothelial cells were prominent in oral SCC, TNBC, and colorectal cancer. Malignant epithelial CCL2 positivity was low: the median donor-level fraction was 1.10%, and the median source contribution was 2.80% across 19 evaluable donors from oral SCC and NSCLC. In UPS, malignant mesenchymal cells had a higher median CCL2-positive fraction (27.9%) and source contribution (25.8%), but this comparison was based on only two UPS donors.

As an independent expression-level validation, five baseline UPS samples from GSE279852 contributed 33,825 cells after QC. Broad marker-based annotation identified mesenchymal/CAF-like, myeloid, endothelial, perivascular, mast, and T/NK compartments. Mesenchymal/CAF-like cells had the largest median CCL2 source contribution (60.7%), and myeloid cells had the highest median CCR2-positive fraction (3.67%). Because the public data lack author cell-type labels, malignant mesenchymal cells and CAF were analyzed together and are reported without a definitive malignant-cell distinction.

CCR2 is sparse and immune-biased

CCR2 was detected in 1,166 of 134,809 carcinoma cells (0.865%) and in approximately 0.34% of UPS cells (Figure 3). The highest donor-level CCR2 fractions were observed in B/plasma, myeloid, and T/NK cells. Malignant epithelial, fibroblast/CAF, and endothelial cells had near-zero CCR2 positivity. The sparsity of CCR2 had two consequences. First, standard LIANA full-network analysis filtered the CCL2-CCR2 axis in all five

cohorts at expr_prop = 0.1, so targeted analysis was required. Second, CellChat required a sparse-receptor thresholding adjustment to retain a non-zero signal.

Stromal-to-myeloid communication is reproducible across lineages

Targeted LIANA identified positive CCL2-CCR2 communication scores for fibroblast/CAF-to-myeloid and endothelial-to-myeloid axes in all five cohorts (Figure 4). Donor-level replication was incomplete but directionally consistent: for example, the endothelial-to-myeloid axis was positive in 10/14 colorectal cancer donors, 5/5 NSCLC donors, and all evaluable donors in the smaller cohorts. Independent CellChat analysis recovered the same two axes in all five cohorts. Perivascular-to-myeloid signaling was also detected in TNBC, colorectal cancer, and NSCLC, indicating that the stromal source is not identical across diseases.

In the GSE279852 baseline validation, simple donor-level pair scores were positive in 5/5 mesenchymal/CAF-to-myeloid and 5/5 endothelial-to-myeloid comparisons and 4/4 perivascular-to-myeloid comparisons. Targeted LIANA was positive in 5/5 fibroblast/CAF donors (3/5 with permutation $p < 0.05$), 5/5 endothelial donors (2/5 below $p < 0.05$), and 4/4 perivascular donors (3/4 below $p < 0.05$). This independent cohort therefore supports the direction of the stromal-to-myeloid axes while retaining annotation and treatment-trial caveats.

Endothelial NFKB_TARGETS is the most stable patient-level CCL2-associated program

In donor-level pseudobulk analysis, endothelial NFKB_TARGETS was positively associated with endothelial CCL2 expression across four datasets (32 donors; pooled rho = 0.680, 95% CI 0.372-0.853, p = 0.00021, I2 = 0) (Figure 5). Myeloid cells showed a smaller positive association (pooled rho = 0.489, p = 0.017, I2 = 0.18). The CAF estimate was very high but unstable (pooled rho = 0.954, I2 = 0.94), so it was not treated as a reproducible patient-level result. The use of CCL2-positive fraction instead of mean CCL2 expression preserved the endothelial and myeloid directions.

Myeloid IL1B is a consistent upstream candidate, whereas TNF is heterogeneous

NicheNet ranked myeloid IL1B in the endothelial NFKB_TARGETS top 20 in 5/5 cohorts (median rank 11, median corrected AUPR 0.300, CCL2 regulatory potential 0.215) (Figure 5). Donor-level myeloid IL1B expression was positively associated with endothelial NFKB_TARGETS (31 donors; pooled rho = 0.452, 95% CI 0.038-0.734, p = 0.0335, I2 = 0). The association with endothelial CCL2 was directionally positive but did not reach the predefined threshold (rho = 0.392, p = 0.071).

Although TNF also ranked highly in NicheNet, donor-level results were contradictory (pooled rho = -0.931, I2 = 0.97 to endothelial NFKB_TARGETS), consistent with severe between-dataset heterogeneity. We therefore retained TNF as an important negative control and did not treat the NicheNet ranking alone as patient-level evidence.

Spatial NF-kB-high regions are myeloid-enriched, but CCL2 is not axis-specific

Across 12 Visium samples, NFKB_TARGETS-high regions had positive neighborhood myeloid correlations in all 12 samples (median rho = 0.324) (Figure 6). Translation null models reached $p < 0.05$ in 6/12 samples; the effect was therefore directionally consistent but only partially robust to spatial permutation. The association with neighborhood CCL2 was weaker and significant under translation nulls in only 2/12 samples.

Control chemokine axes showed that CCL2 was not uniquely coupled to NF-kB-high neighborhoods. Median neighborhood correlations were 0.173 for CXCL9, 0.170 for CXCL8, 0.170 for CCL5, 0.151 for CXCL10, and 0.130 for CCL2. Marker-based compartment scores identified myeloid cells as the compartment most consistently enriched with NFKB_TARGETS in sarcoma, treated ccRCC, and squamous carcinoma. Spatial proximity therefore supports a myeloid-associated NF-kB state but does not establish CCL2 specificity or direct communication.

Microenvironment targets are more plausible than direct tumor-cell NF-kB inhibition

DepMap 24Q4 showed near-zero mean gene effects for IL1B, IL1R1, IL1RAP, CCL2, CCR2, TNF, TNFRSF1A, TNFRSF1B, NFKB1, and IKBKB (Supplementary Figure S4). RELA had a more negative mean effect (-0.406), but this effect was broad and not sarcoma-selective. PRISM 24Q2 showed weak single-agent

activity for most CCR2 and specific NF-kB compounds; the strongest IKK/NF-kB hit, BX-795, is multi-target and cannot be interpreted as NF-kB-specific.

In TCGA-SARC UPS, higher NFKB_TARGETS was associated with better OS (HR = 0.035, 95% CI 0.0033-0.382, p = 0.0059) and DFS (HR = 0.104, 95% CI 0.023-0.477, p = 0.0036). NFKB_CORE showed the same direction. Individual CCL2, IL1B, IL1R1, and CCR2 genes were not significantly associated with survival. After adjustment for endothelial and myeloid deconvolution fractions, NFKB_TARGETS remained protective for OS (p = 0.017) and DFS (p = 0.025), although the five-fraction DFS model was not significant. These findings suggest that the bulk NFKB_TARGETS score captures an immune/stromal context rather than a tumor-intrinsic adverse program.

In the independent GSE202361 immune checkpoint blockade cohort, higher baseline TNF was associated with lower PD odds after age adjustment (OR = 0.304, 95% CI 0.080-0.857, p = 0.043); CCL2 (OR = 0.343, p = 0.052) and NFKB_CORE (OR = 0.347, p = 0.065) were directionally consistent but did not meet $p < 0.05$. The direction matches the protective TCGA-SARC result. The analysis is limited to 23 baseline samples, eight PD events, no verified histology or treatment arm mapping, and no continuous hyalinization endpoint.

We further tested the expression-level relationships in two external UPS bulk datasets. In GSE75885 (37 UPS samples), NFKB_TARGETS was positively associated with CCL2 (rho = 0.651, p = 1.28e-05) and IL1B (rho = 0.829, p = 2.38e-10). In GSE299349 (14 UPS samples), the corresponding estimates were rho = 0.508 (p = 0.064) for CCL2 and rho = 0.625 (p = 0.017) for IL1B. Fixed-effect meta-analysis across 51 samples yielded pooled rho = 0.619 (95% CI 0.407-0.768, p = 1.20e-06) for NFKB_TARGETS-CCL2 and pooled rho = 0.791 (95% CI 0.654-0.878, p = 5.83e-13) for NFKB_TARGETS-IL1B. After adjustment for leukocyte and stromal expression scores, the NFKB_TARGETS-CCL2 estimate attenuated in both datasets (GSE75885 adjusted rho = 0.304, p = 0.067; GSE299349 adjusted rho = 0.468, p = 0.091), whereas the IL1B association remained directionally positive.

In the GSE285972 human UPS PDX treatment model, UPS2236 showed higher NFKB_TARGETS, IL1B, and IL1R1 at week 3 than in controls (FDR = 0.008, 0.008, and 0.017), but CCL2 did not show a corresponding significant increase (p = 0.284; FDR = 0.650). The replicate-level NFKB_TARGETS-CCL2 association was positive but not significant (rho = 0.451, p = 0.069). MFH9 showed no significant changes across treatment time points. These data indicate that therapy may induce an NF-kB/IL1B state without a proportional CCL2 increase, and they are reported only as a treatment-context sensitivity analysis.

Integrated target priority

The strongest convergent target is myeloid IL1B to endothelial IL1R1, followed by CCL2-CCR2. Endothelial NF-kB remains mechanistically central but is not an attractive systemic drug target because of poor tumor-cell selectivity. TNF is a high-ranking NicheNet ligand but lacks donor-level consistency. CCL2-CCR2 blockade is better positioned as a microenvironment-directed therapy or pharmacodynamic strategy than as a single-agent tumor-cell cytotoxicity strategy.

Discussion

This cross-lineage analysis reframes CCL2 as a multicellular stromal communication node rather than a uniform tumor-cell program. The most reproducible patient-level relationship connected endothelial NFKB_TARGETS to CCL2, with myeloid IL1B as the most consistent upstream ligand candidate. Together with LIANA and CellChat, these results support a model in which myeloid IL1B activates endothelial NF-kB and promotes endothelial CCL2 expression, which can then engage CCR2 on myeloid cells. The model is hypothesis-generating and requires functional perturbation.

The study also produced important negative findings. CCL2 was not more spatially specific than CXCL9, CXCL8, CCL5, or CXCL10. TNF was ranked highly by NicheNet but was not stable at the donor level. Direct NF-kB inhibition lacked selective dependency, and CCR2/NF-kB compounds had weak single-agent activity in cancer cell lines. These results argue against using bulk cell-line sensitivity or cancer-cell dependency as the main rationale for targeting this axis.

The external clinical analyses change the direction of the prognostic narrative. Higher NFKB_TARGETS and NFKB_CORE scores were associated with better survival in TCGA-SARC UPS, and higher baseline CCL2, TNF, and NFKB_CORE were directionally associated with lower PD odds in GSE202361. These findings are consistent with an immune-hot or stromal-rich context and do not support a simple "higher NF-kB equals worse outcome" model. They do not demonstrate that CCL2 is beneficial, because CCL2 is only one component of a complex inflammatory program and may have opposing effects at different disease stages. The external UPS bulk replication confirms an expression-level NF-kB-CCL2 and NF-kB-IL1B relationship, while also showing that the CCL2 association is partly explained by leukocyte and stromal composition. The GSE285972 PDX analysis further cautions that chemotherapy-associated induction of NF-kB and IL1B does not necessarily increase CCL2.

The primary UPS discovery comparison remains based on two donors and should be treated as provisional. An independent GSE279852 baseline cohort adds five UPS donors and supports the stromal-to-myeloid direction, but it comes from a single treatment trial and uses broad marker-based annotation. CCR2 is sparse, making communication inference sensitive to normalization and threshold choices. Spatial spots contain multiple cells, and spatial proximity is not direct communication. The patient-level analyses are observational, with residual confounding by treatment, tissue composition, and disease context. TCGA-SARC contains only 44 UPS-like tumors, and the deconvolution reference is derived from the same two UPS donors. GSE202361 has 23 baseline samples and no verified crosswalk to the continuous pathology endpoint. NicheNet, LIANA, and CellChat are inference methods, not causal evidence.

The next experimental step should test whether IL1B stimulation of endothelial cells increases NF-kB-dependent CCL2 secretion and whether IL1R1, NF-kB, or CCR2 blockade reduces myeloid migration. The validation should use endothelial-myeloid co-culture or Transwell assays, with IL1B as the primary ligand candidate and TNF as a mechanistic but unstable comparator.

Figure legends

Figure 1. Study design and candidate communication model. Five single-cell cohorts, 12 spatial samples, and external bulk validation datasets were integrated with communication, patient-level, upstream-ligand, dependency, and clinical analyses. The model summarizes the main reproducible route: myeloid IL1B to endothelial NF-kB and CCL2, followed by CCR2-dependent myeloid recruitment.

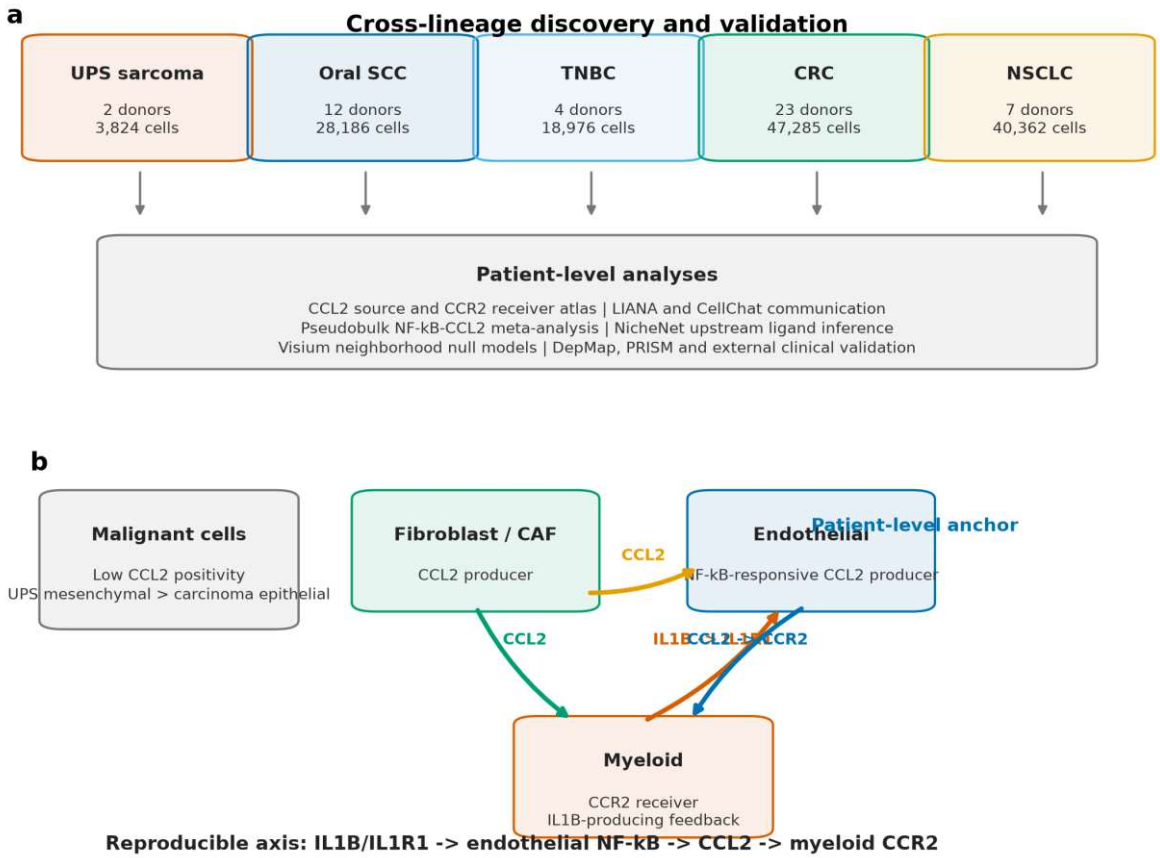


Figure 2. CCL2 source landscape. Donor-level CCL2 positivity by disease and harmonized cell type, pooled source contribution, and malignant-cell positivity in UPS and carcinoma cohorts.

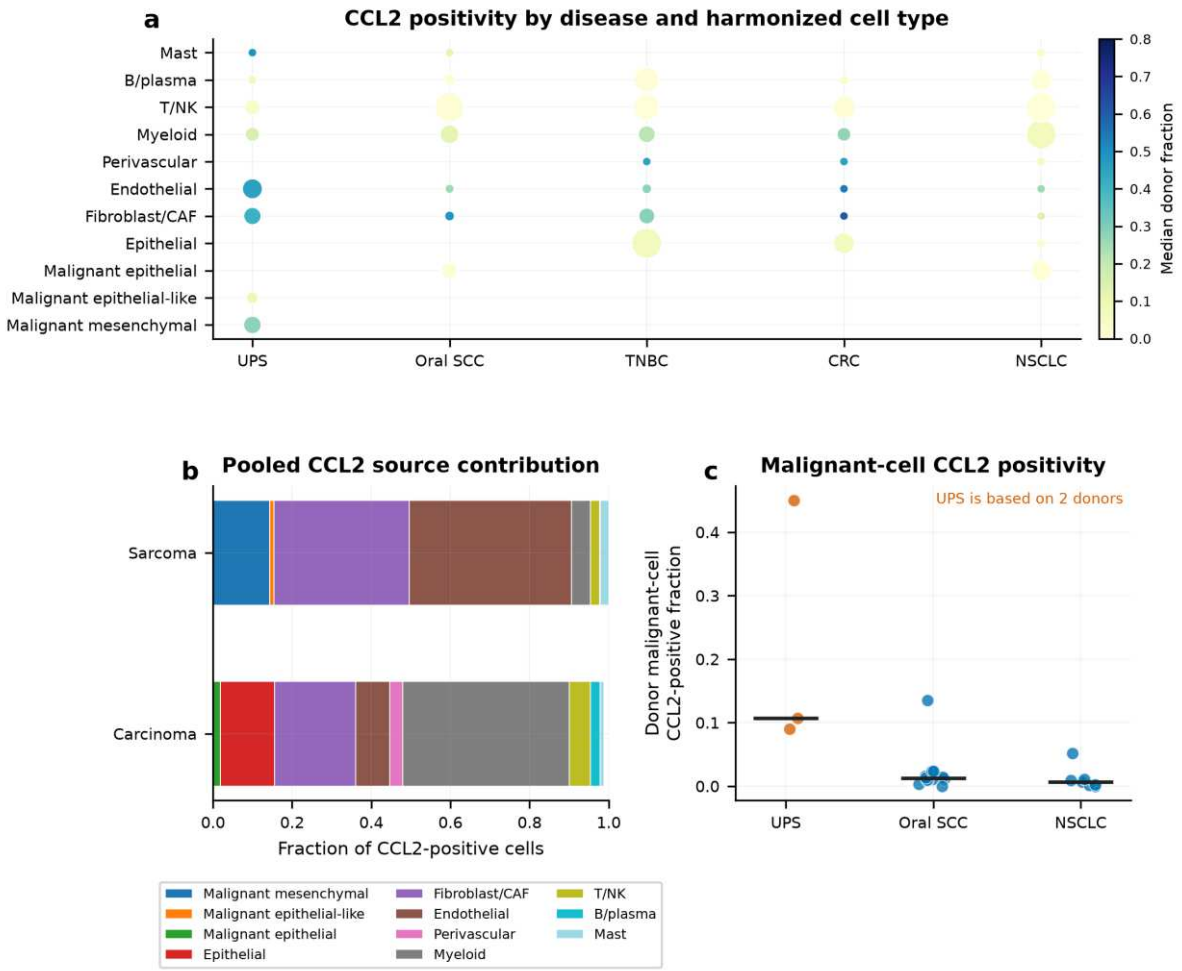


Figure 3. CCR2 receiver landscape. Donor-level CCR2 positivity, total CCR2-positive cells by compartment, and the principal CCR2-positive immune compartments.

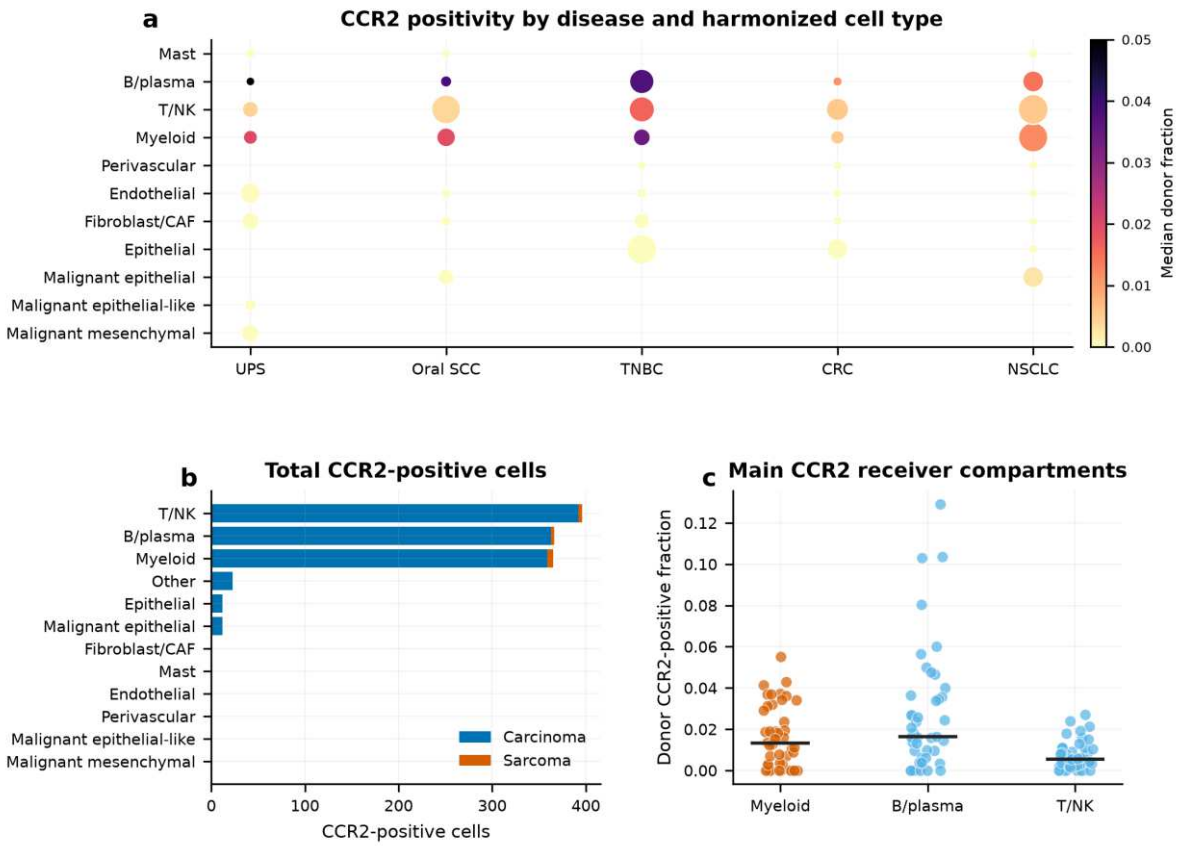


Figure 4. CCL2-CCR2 communication axes. LIANA scores, donor-level positive fractions, and independent CellChat probabilities for stromal-to-myeloid axes across cohorts.

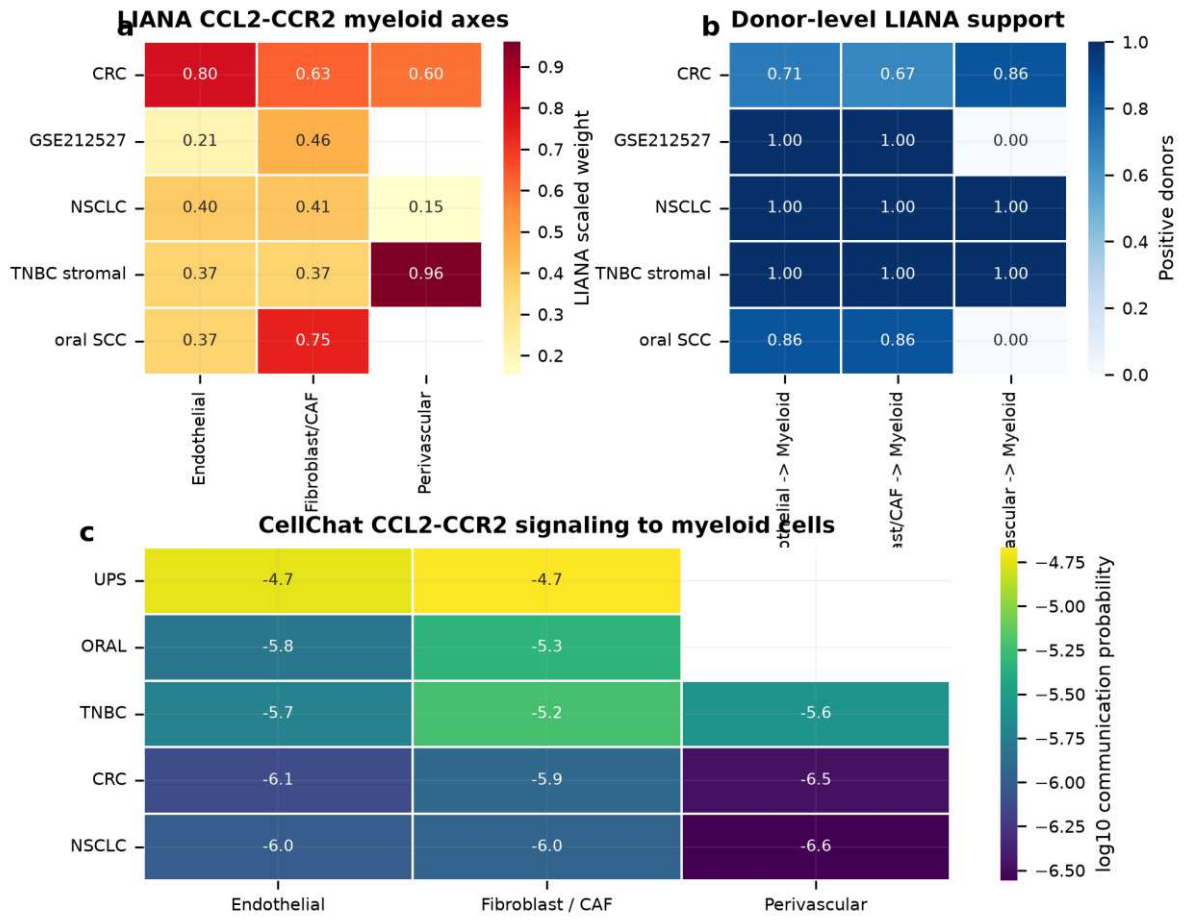


Figure 5. Patient-level NF-kB, CCL2, and upstream ligand evidence. Pseudobulk meta-analysis, endothelial donor-level association, NicheNet endothelial ligand ranking, and donor-level IL1B/TNF consistency.

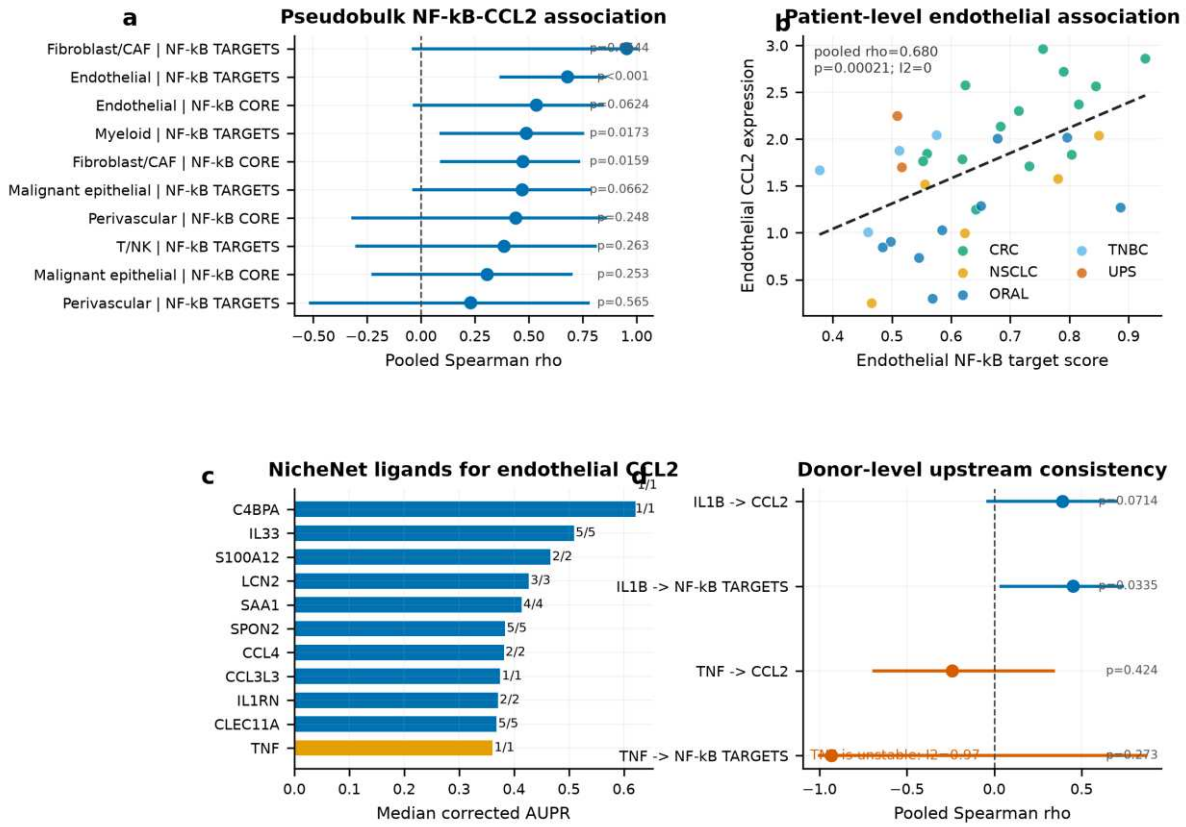
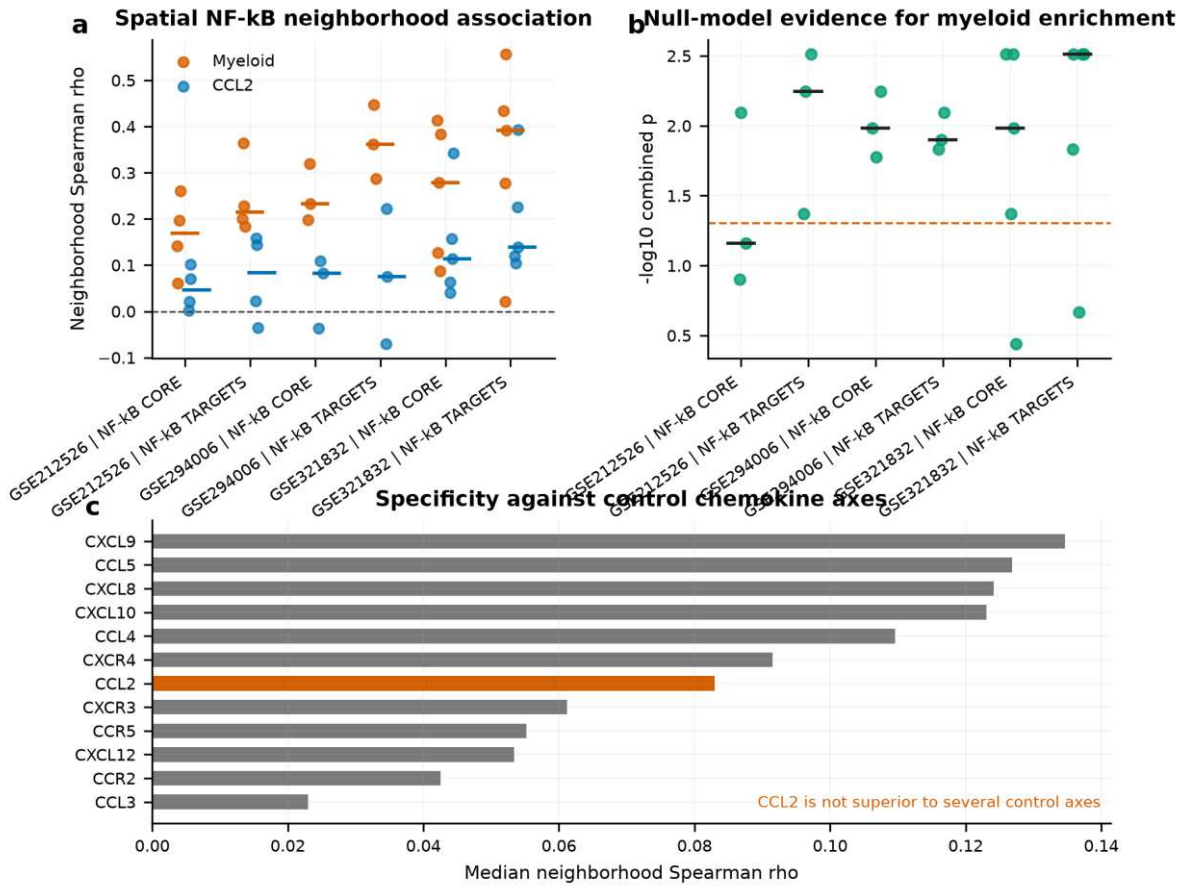


Figure 6. Spatial validation. Neighborhood associations, spatial null-model significance, and control chemokine axes. The figure shows that myeloid enrichment is more consistent than CCL2 specificity.



Supplementary Figure S4. Target prioritization. DepMap cell-autonomous dependency, PRISM compound sensitivity, external TCGA-SARC and GSE202361 validation, and the final target priority matrix. Supplementary Figure S1 shows the GSE75885 and GSE299349 UPS bulk replication.

Supplementary Figure S1. External UPS bulk validation in GSE75885 and GSE299349. Supplementary Figure S2. GSE285972 UPS PDX treatment-context sensitivity analysis. Supplementary Figure S3. GSE279852 UPS baseline single-cell validation. Supplementary Table S1. Cohort and dataset inventory. Supplementary Table S2. Integrated target-prioritization matrix.

Author contributions

Saiyang Li: Conceptualization; Methodology; Software; Validation; Formal analysis; Investigation; Data curation; Writing - original draft; Writing - review and editing; Visualization; Project administration.

Funding

This research received no external funding.

Competing interests

The author declares no competing interests.

Ethics statement and consent

This study used public de-identified human datasets. The source studies are responsible for their original ethics approvals and consent procedures. This secondary analysis did not require new participant contact.

Consent for publication is not applicable because no identifiable participant-level material or images are presented.

Data and code availability

Public source datasets are identified by GEO or CELLxGENE accession in the Methods. All source datasets are publicly available through the accessions listed in the manuscript. Derived tables and figure source data are included in the supplementary files. Analysis code is included as Supplementary Code with the manuscript.

AI-use disclosure

OpenAI Codex was used to assist with code generation, data processing, statistical analysis, figure preparation, and manuscript drafting. The author reviewed and verified all analyses, numerical results, citations, and text, and takes full responsibility for the final manuscript.

References

1. Jin Y, Wang Y, Yang R. Chemokine ligand 2: beyond chemotaxis - a multifaceted role in tumor progression. Frontiers in Immunology. 2025. doi:10.3389/fimmu.2025.1685474.

2. Chen X, Zhou J, Wang Y, et al. PIM1/NF-kB/CCL2 blockade enhances anti-PD-1 therapy response by modulating macrophage infiltration and polarization in the tumor microenvironment of NSCLC. Oncogene. 2024. doi:10.1038/s41388-024-03100-6.

3. Roland CL, Nassif Haddad EF, Keung EZ, et al. A randomized, non-comparative phase 2 study of neoadjuvant immune checkpoint blockade in retroperitoneal dedifferentiated liposarcoma and extremity/truncal undifferentiated pleomorphic sarcoma. Nature Cancer. 2024;5:625-641. doi:10.1038/s43018-024-00726-z.

Supplementary Files

This is a list of supplementary files associated with this preprint. Click to download.

- figS2gse285972pdxtreatment.tiff
- figS1externalupsvalidation.tiff
- figS4targetprioritization.tiff
- figS3gse279852upsvalidation.tiff